

1 incorporated in the hybrid nanofibers and only was needed to 0.43 wt% of GO increase the conductivity
2 of the CA-[BMIM]Cl nanofibers by more than four orders of magnitude (from 2.71×10^{-7} S/cm to
3 5.30×10^{-3} S/cm). This ultra-high enhancement opens up a new route for conductive enhancement of
4 biopolymer nanofibers to be used in smart (bio) electronic devices.

5 **1. Introduction**

6 Enormous volumes of synthetic polymers accumulating in the natural environment has become
7 a major threat to the planet due to their poor degradability and high CO₂ footprint. In response
8 to this growing concern, the past decade has seen a considerable interest in the replacement of
9 synthetic polymers with biopolymers owing to their abundance in nature and excellent
10 biocompatibility and biodegradability [1]. In parallel, biopolymeric nanofibrous fabrics can
11 deliver superior performance in terms of functionality and degradability due to their high
12 surface area-to-volume ratio. Electrospinning has been shown to be a versatile method for
13 fabricating nanofibers from a wide range of polymers, allowing the facile incorporation of
14 additives, such as drugs, nanoparticles or nanofillers to produce hybrid nanofibrous materials
15 for a wide range of applications (*e.g.* as therapeutic, protective, electrical or sensing materials)
16 [2-7]. Developing functionalized polymer materials such as conductive nanofibers from
17 abundant and biodegradable biopolymers is more challenging and has attracted an increasing
18 amount of attention for the benefit of energy utilization and the environment [1]. A number of
19 synthetic polymers, such as poly(vinyl alcohol) (PVA), polyacrylonitrile (PAN), polyaniline
20 (PANI) and poly(vinyl pyrrolidone) (PVP), have been successfully combined with graphene
21 sheets and carbon nanotubes to produce conductive nanofibers [8, 9]. However, very few
22 contributions have been made to the electrospinning of biopolymers with carbon nanotubes or
23 graphene. Of these contributions, carbon nanotubes are more popular and have been
24 successfully electrospun with biopolymers such as chitosan, cellulose triacetate and
25 biodegradable polylactide [10-12]. Graphene (layered sp²-hybridized honeycomb lattice

1 carbon sheets) has gained particular interest owing to its multifunctional properties such as
2 high specific surface area, electrical and thermal conductivity and superior mechanical strength
3 [13]. Most pertinently, the excellent electrical properties of graphene renders it a promising
4 nanomaterial for novel practical applications such as smart fabrics, nanosensors and flexible
5 electrode materials [14, 15].

6 Producing graphene/biopolymer nanofibers by electrospinning has three distinct challenges: 1)
7 disrupting the extensive hydrogen bonding within the biopolymer; 2) breaking the aggregation
8 of the graphene sheets into nanoparticles to prepare a uniform mixture for electrospinning; and
9 3) establishing appropriate interactions in the hybrid material to facilitate electron transport. A
10 dispersing agent is required to break-up the graphene sheets due to its inherent insolubility,
11 atomically smooth surfaces and strong aggregation tendency. Choosing an appropriate
12 dispersing agent therefore becomes the key to formulating spinnable mixtures to fabricate
13 hybrid biopolymer nanofibers. Ionic liquids (ILs) present an interesting class of reagents that
14 can be used as dispersing agents because of their novel dissolution ability and have the potential
15 to play more functional roles such as stabilizers, compatibilizers, modifiers and additives in the
16 fabrication of polymer composites containing carbon nanotubes or graphene sheets [16]. ILs
17 are organic salts which exist in the liquid state below 100°C, preferably at room temperature,
18 and offer chemical and thermal stability, non-flammability and immeasurably low vapor
19 pressure [17, 18].

20 Imidazolium chloride-based ILs show outstanding dissolving capacity of many biopolymers
21 such as cellulose, cellulose acetate, chitin, wool and chitosan. The high chloride concentration
22 of the IL breaks the extensive hydrogen-bonding network of these biopolymers to enable
23 successful electrospinning [18-25]. In such ILs, graphene oxide sheets can be effectively
24 exfoliated, stabilized and reduced by chemical and thermal treatment methods [26, 27]. Peng

1 and colleagues fabricated graphene-cellulose nanocomposite films successfully by casting,
2 through the exploitation of imidazolium chloride-based ILs [28]. These cast films showed
3 conductivities up to 3.2×10^{-2} S/cm, thus demonstrating an approach for ionic liquid-
4 biopolymer conductive nanocomposites with graphene. Further, the use of IL, 1-butyl-3-
5 methylimidazolium chloride ([BMIM]Cl, 20%), in the production of electrospun hybrid carbon
6 nanotube nanofibers with styrene-acrylonitrile resin showed a significant increase in the
7 conductivity from 1.08×10^{-6} S/cm to 5.9×10^{-6} S/cm for samples containing 3 wt% carbon
8 nanotubes [29]. However, the fabrication of electrospun graphene-biopolymer conductive
9 nanofibers remains a significant challenge.

10 In the first report of its kind, we present an electrospinning study of cellulose acetate
11 (biopolymer), graphene oxide (source of graphene) and [BMIM]Cl (ionic liquid) to create
12 hybrid nanofibers. A chemical reduction method using hydrazine in an ultrasound humidifier
13 has been developed to reduce graphene oxide to enhance the electrical conductivity of the
14 biopolymer nanofibers. Scanning Electron Microscopy (SEM), X-ray Diffraction (XRD) and
15 Raman, Fourier Transform Infrared (FTIR) and X-ray Photoelectron (XPS) spectroscopies
16 have been used extensively to probe the interactions within our novel hybrid nanofibers.

17 **2. Experimental**

18 *2.1. Materials*

19 1-Methylimidazolium (99%), ethyl acetate (99%) and 1-chlorobutane (99%) were purchased
20 from Merck. CA powder ($M_n = 30,000$ Da, acetyl content 39.8 %), acetone, dimethylacetamide
21 (DMAc) and hydrazine solution (35 wt% in H₂O), all from Sigma Aldrich, were used as
22 received. Graphene oxide powder (15-20 sheets, 4-10% edge-oxidized) was purchased from
23 Garmor Inc. U.S.A. 1-Butyl-3-methylimidazolium chloride [BMIM]Cl was synthesized by the
24 method described elsewhere [30].

1 2.2. Preparation CA and [BMIM]Cl-GO blends

2 First, a 17 wt% CA solution was prepared in 2:1 (w/w) acetone/DMAc at room temperature
3 under constant stirring until a homogenous, transparent solution was obtained. [BMIM]Cl-GO
4 solutions were prepared by adding a given amount of GO (0.11-0.43% by weight of CA) to
5 [BMIM]Cl (12% by weight of CA) under constant stirring at 60 °C for 24 h. Finally,
6 [BMIM]Cl-GO was added to the CA solution and stirred at room temperature for a further 2 h
7 (experimental details given in the Supporting Information). This solution, denoted as CA-
8 [BMIM]Cl-GO throughout this work, was then ready for electrospinning.

9 2.3. Electrospinning of CA-[BMIM]Cl-GO nanofibers

10 Solutions for electrospinning were loaded into a 1 mL syringe with a stainless-steel needle
11 (0.6 mm inner diameter). Electrospinning was performed at room temperature in a horizontal
12 geometry with an applied voltage of 20-25 kV (Gamma High Voltage Research power supply,
13 ES 40R-20W/DM/M1127 Ormond Beach FL). The flow rate of the solution was fixed at
14 1.5 mL/h using a syringe pump (NE-1010 Programmable Single Syringe Pump, New Era Pump
15 Systems, Inc). The distance between the needle tip and the collector was maintained at 8-
16 10 cm. CA-[BMIM]Cl-GO nanofibers were continuously deposited onto an electrically
17 grounded rotatory collector covered with aluminum foil. The CA-[BMIM]Cl-GO hybrid
18 nanofibers were then carefully removed from the aluminum foil and dried at room temperature
19 for 24 hours.

20 2.4. Preparation of CA-[BMIM]Cl-rGO nanofibers

21 To reduce the oxygen content of the GO to create electrically conductive nanofibers, CA-
22 [BMIM]Cl-GO nanofibrous mats were reduced by a hydrazine solution mist [31, 32]. In short,
23 the hydrazine solution was placed in an ultrasound humidifier (BONECO Ultrasonic U7146,

1 Switzerland). The fibrous mats were clamped in a universal extension retort clamp in the front
2 of the humidifier at maximum humidity (see supplementary video in the supporting
3 Information) for 15-30 minutes until the mats changed into the typical black graphitic color.
4 Following reduction, the mats were allowed to dry at room temperature for 2 h to give
5 CA-[BMIM]Cl-rGO nanofibers.

6 *2.5. Characterization*

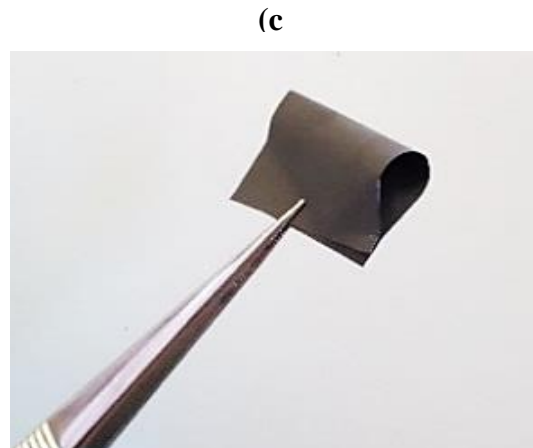
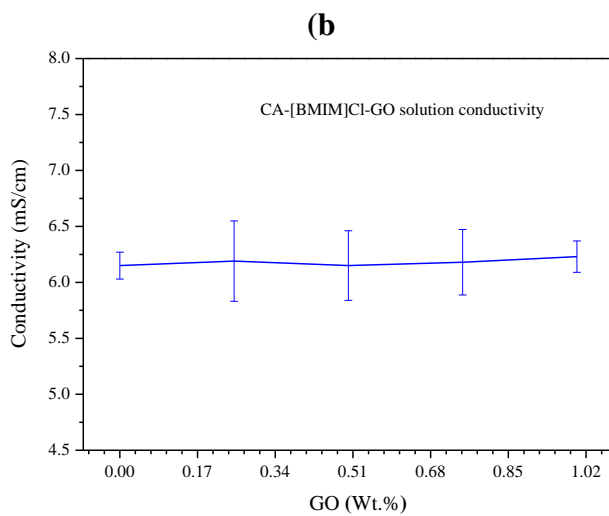
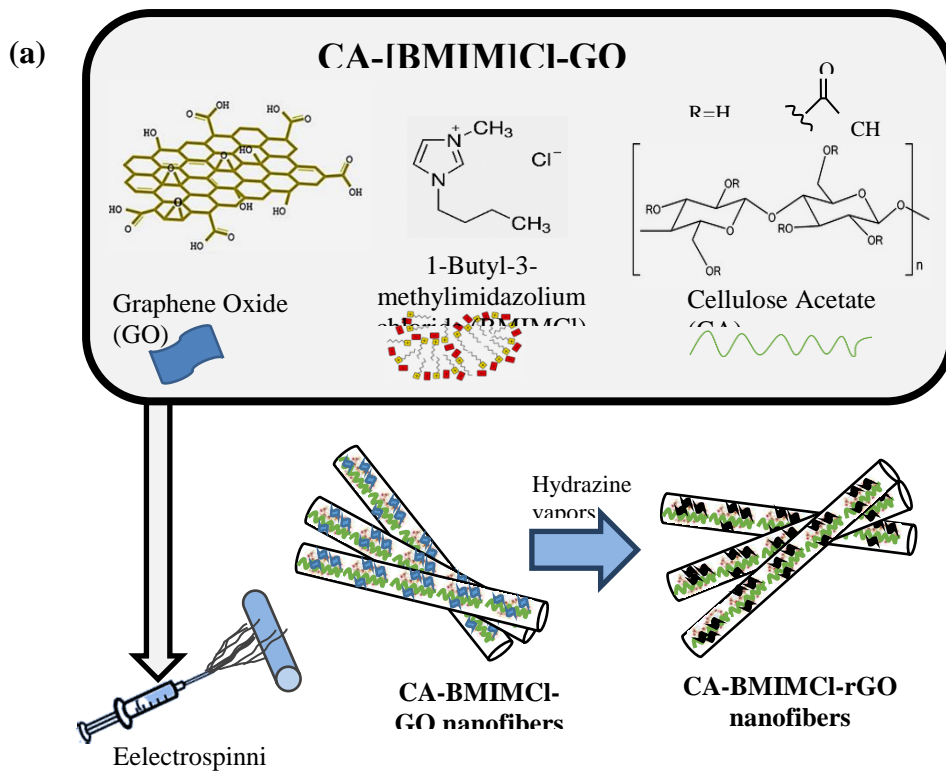
7 The surface morphologies of the nanofibers were analyzed by scanning electron microscopy
8 (SEM, Zeiss FEG-SEM Ultra-55) and intermolecular interactions within the nanofibrous mats
9 were analyzed by FTIR (Interspec 200-X) spectroscopy. The thickness of the mats was
10 measured by a Mitutoyo Mischecker M519-402 micrometer and the approximate porosity of
11 the final electrospun nanofibrous mats was calculated by image analysis, as described in the
12 Supporting Information. Chemical states and surface composition were characterized by X-ray
13 photoelectron spectroscopy (XPS, Kratos AXIS Ultra DLD X-ray Photoelectron
14 Spectrometer). Raman spectroscopy (Renishaw inVia Raman spectrometer) was used to probe
15 the surface composition and X-ray diffraction (XRD) patterns were recorded by a Rigaku
16 Ultima IV diffractometer with Cu K α radiation ($\lambda = 1.5406 \text{ \AA}$, 40 kV at 40 mA) using a silicon
17 strip detector D/teX Ultra with the scan range of $2\theta = 5.0 - 30.0^\circ$, scan step 0.02° , scan speed
18 $5^\circ/\text{min}$. The electrical conductivities of the solutions were analyzed using a conductivity meter
19 (SevenCompactS230 Mettler Toledo, Switzerland) at room temperature while the conductivity
20 of the nanofiber mats was measured using a two-probe method with an AlphaLab, Inc.
21 multimeter by placing the mats between two gold electrodes at a separation of 1 cm. The
22 thermal stability of CA, CA-[BMIM]Cl, CA-[BMIM]Cl-GO and CA-[BMIM]Cl-rGO
23 nanofibers was analyzed using Thermogravimetric Analysis (TGA, Setaram LabsysEvo 1600
24 thermo analyzer) under argon between 25°C to 700°C at a heating rate of $10^\circ\text{C}/\text{min}$.

1 **3. Results and discussion**

2 *3.1 The morphology and the conductivity of the hybrid nanofibers*

3 A schematic of the preparation method of CA-[BMIM]Cl-rGO nanofibers is presented in
4 Figure 1a, where GO was first dispersed in [BMIM]Cl and then mechanically mixed in a
5 solution of CA. Dispersing GO into [BMIM]Cl was carried out by magnetic stirring at
6 approximately 60 °C to ensure that the ionic liquid had fully melted. As the melt has a viscosity
7 larger than 150 mPa·s [33], mixing was performed for 24 hours to ensure dispersion of the GO
8 nanoparticles in [BMIM]Cl, which is a critical step for successful electrospinning. The CA-
9 [BMIM]Cl-GO solution was electrospun prior to reduction by hydrazine mist using an
10 ultrasound humidifier. Compared to other chemical reduction methods [31, 32], our ultrasound
11 reduction method by hydrazine mist significantly reduces GO at a lower temperature (room
12 temperature) than previously reported in the literature [31, 32, 34]. This provides a new method
13 to easily control the reduction process for highly conductive graphene-based nanofibers. The
14 conductivity of the CA-[BMIM]Cl solution (prior to the incorporation of GO) was measured
15 at 6.23 mS/cm and remained almost constant (Figure 1b) as the amount of GO increased from
16 0.11 to 0.43 wt%. This is due to the presence of oxygenated groups on the surface of GO which
17 disrupts the sp² hybridization in graphene. Produced nanofibers with controlled amounts of GO
18 in the range of 0 - 0.43 wt% are shown in Table 1. Pure CA, CA-[BMIM]Cl, CA-[BMIM]Cl-
19 GO and CA-[BMIM]Cl-rGO nanofibers were then examined by SEM. Surface morphologies
20 of CA, CA-[BMIM]Cl and CA-[BMIM]Cl-GO (see Figure 2a and b) were smooth and bead-
21 free, while CA-[BMIM]Cl-rGO nanofibers have rough regions where GO appears to have
22 aggregated (as shown in Figure 2d). Higher concentrations of GO hindered the jet flow due to
23 excess GO, which was not fully dispersed in the solution, clogging the needle and therefore
24 electrospinning was unsuccessful. During chemical reduction, the CA-[BMIM]Cl-GO

1 nanofibers became more fused (Figure 2d) to form a CA-[BMIM]Cl-rGO nanofibrous mat. The
2 conductivity of CA-[BMIM]Cl nanofibers was measured at 2.71×10^{-7} S/cm, which was
3 significantly lower than the conductivity of pure [BMIM]Cl *i.e.* 4.60×10^{-4} S/cm [35].
4 Incorporation of GO resulted in an increase in the conductivity of the nanofibers, before and
5 after the reduction. For non-reduced nanofibers, the presence of GO (0.11 wt%) increased the
6 conductivity (to 4.33×10^{-5} S/cm) and reaching an approximate plateau at 1.41×10^{-4} S/cm at
7 0.43 % GO. The conductivity of the nanofibers is presented in Table 1 and Figure 3.
8 Comparing to GO/CA nanocomposites reported in the literature, [34] 0.43 wt% GO is a
9 relatively low loading for such a significant conductivity enhancement.

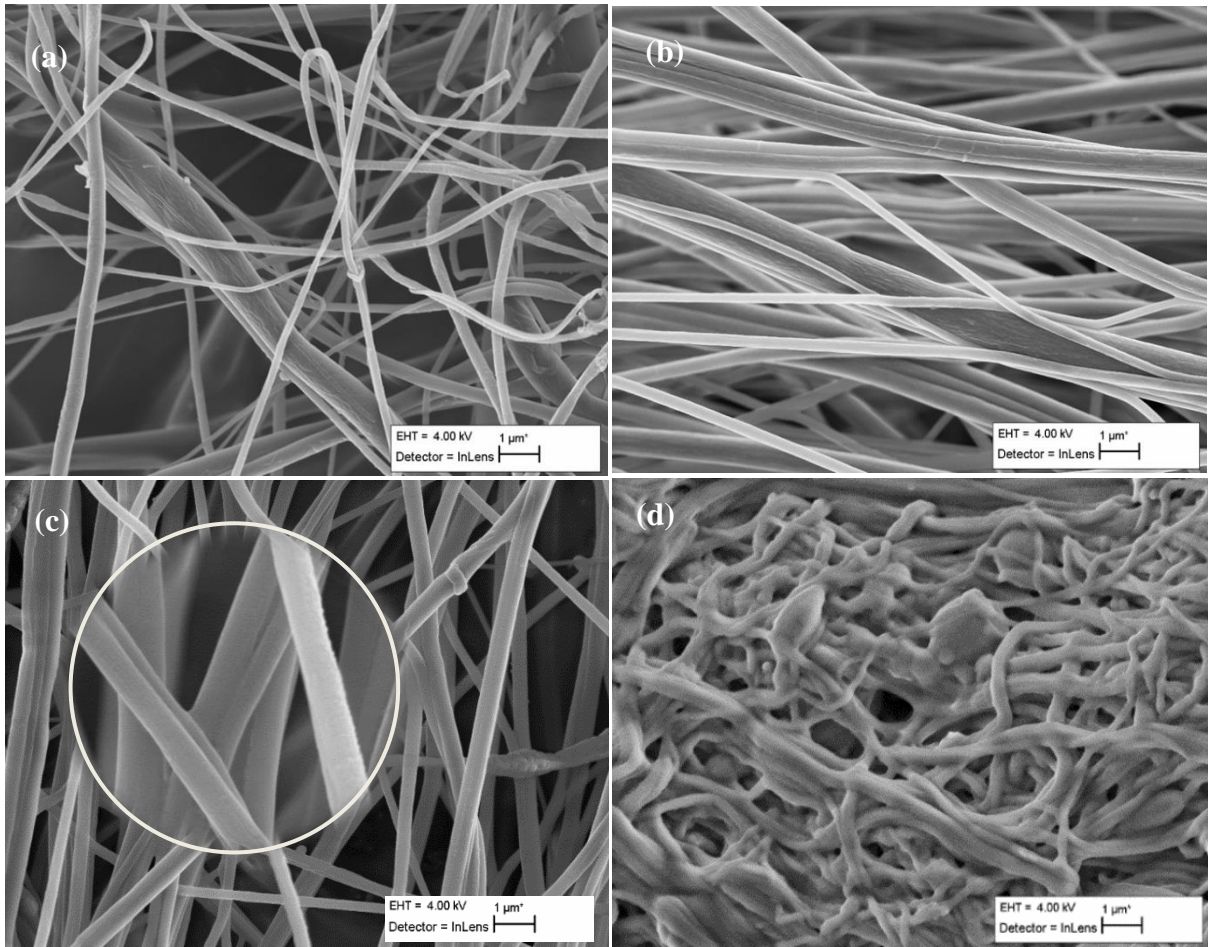


1

2 **Figure 1** (a) Schematic of the preparation of CA-[BMIM]Cl-rGO nanofibers, (b) Influence of

3 GO concentration on the conductivity of the CA-[BMIM]Cl solution and (c) a photographic

4 image to demonstrate the flexibility and durability of the final hybrid nanofibrous material.



1

2

Figure 2 SEM images of (a) pure CA; (b) CA-[BMIM]Cl; (c) CA-[BMIM]Cl-GO and (d) CA-[BMIM]Cl-rGO(GO conc. 0.43 wt%) nanofibers.

3

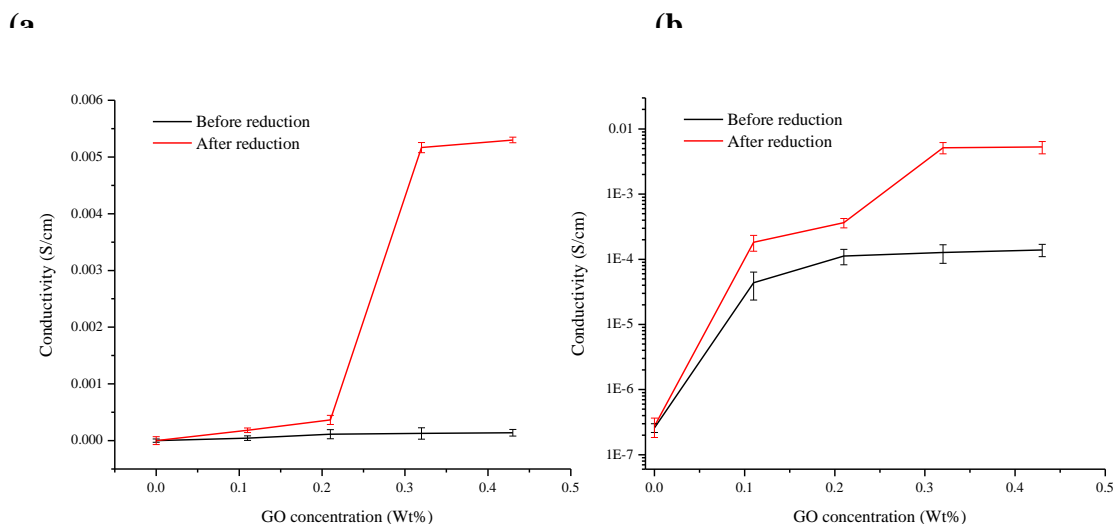
4

5

Table 1 Conductivity of the hybrid CA-[BMIM]Cl-rGO nanofibers.

Content, wt%			Conductivity (S/cm)	
GO	[BMIM]Cl	CA	before reduction	after reduction
0.00	46.60	53.40	2.71×10^{-7}	2.71×10^{-7}
0.11	46.50	53.39	4.33×10^{-5}	1.82×10^{-4}
0.21	46.41	53.38	1.11×10^{-4}	3.65×10^{-4}
0.32	46.31	53.37	1.29×10^{-4}	5.10×10^{-3}
0.43	46.21	53.36	1.41×10^{-4}	5.30×10^{-3}

6



1

2 **Figure 3** The effect of GO concentration in the hybrid CA-[BMIM]Cl-GO nanofibers on
 3 conductivity [(a) linear and (b) log scales] before and after reduction.

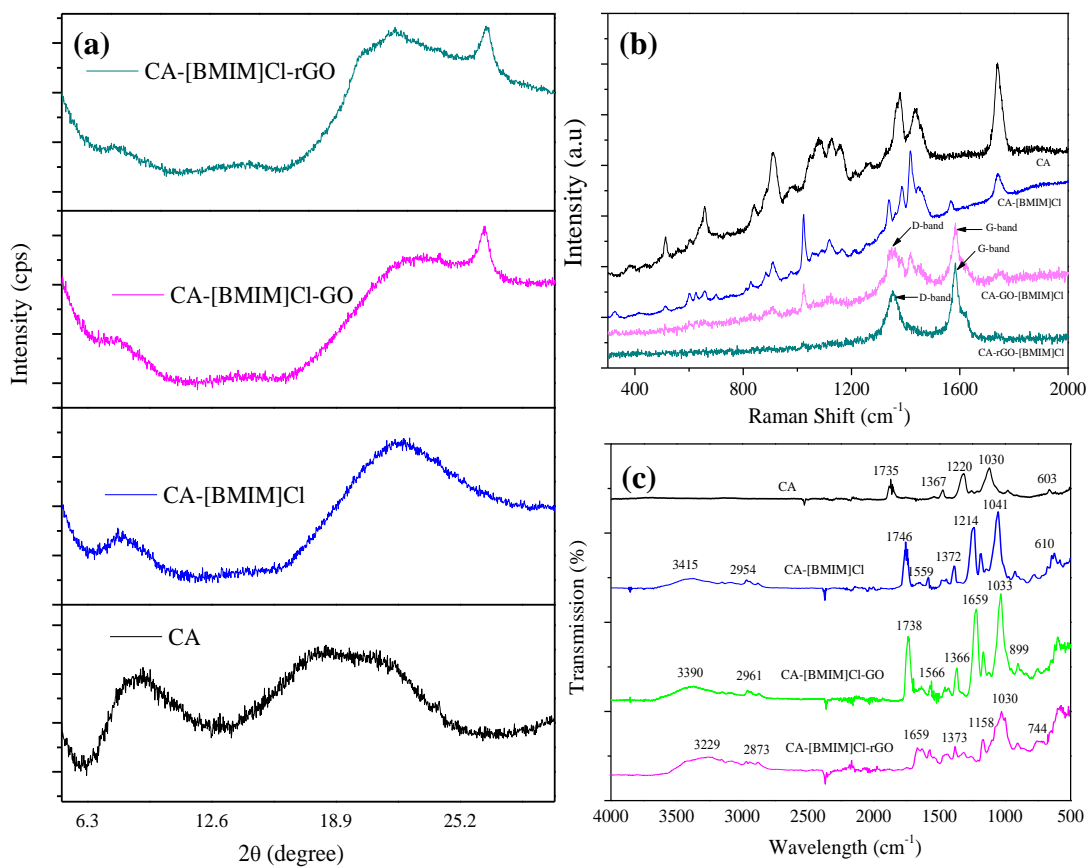
4 Interestingly, reduction of the hybrid nanofibers using hydrazine boosted the conductivity
 5 significantly, surpassing the conductivity of pure [BMIM]Cl when GO loading reached 0.32
 6 wt% (4.60×10^{-4} S/cm). The highest conductivity attained was 5.30×10^{-3} S/cm with 0.43 wt%
 7 GO, which is $\sim 20,000$ times higher than that of the nanofibers without GO and over an order
 8 of magnitude higher than that of pure [BMIM]Cl.

9 3.2. Structure of graphene oxide in the nanofibers

10 X-ray diffraction (XRD) was used to examine the crystal structure of CA and GO following
 11 the electrospinning and reduction processes. The XRD patterns of the CA, CA-[BMIM]Cl,
 12 CA-[BMIM]Cl-GO and CA-[BMIM]Cl-rGO nanofibers are shown in Figure 4a. Pure CA
 13 nanofibers exhibited three broad diffraction peaks at 9.0° , 17.9° and 21.8° [36]. The peak at
 14 21.8° is attributed to short-range spacing between neighboring cellulosic repeat units within
 15 the individual macromolecules and the peak at 9.0° shows the longer range interactions
 16 between cellulose acetate chains [37]. More specifically, the distance between the adjacent
 17 cellulosic chains is normally characterized by a d-spacing of $\sim 9 - 10 \text{ \AA}$, and the neighboring

1 anhydroglucose units in the cellulose chains have a d-spacing of $\sim 4 - 5.5 \text{ \AA}$. The peak at 17.9°
2 could arise from the diffraction of the (021) plane. After addition of [BMIM]Cl, the peak at
3 9.0° became significantly weaker and shifted to 8.0° . This peak weakening and shifting to a
4 lower angle reflects the decrease in CA concentration in the nanofibers from 100% to 53.4%
5 and the cellulose packing disrupted by [BMIM]Cl. The presence of [BMIM]Cl breaks up the
6 H-bonding between the cellulosic chains and enlarges their d-spacing from 9.8 \AA to 11.0 \AA . A
7 small shift of the 21.8° peak is also observed, illustrating that the addition of [BMIM]Cl did
8 not significantly alter the anhydroglucose units in the cellulose acetate chain. The peak at 17.9°
9 almost completely disappeared from the nanofiber samples electrospun in the presence of
10 [BMIM]Cl, showing less short range order in the amorphous cellulose acetate. The addition
11 of 0.11 wt% GO resulted in the appearance of a sharper peak at $\sim 26.5^\circ$, which is the (002) peak
12 of graphite. The (002) peak shows that the interlayer spacing of the graphite sheets was
13 approximately 0.33 nm (3.3 \AA).

14 This suggests that the graphene sheets are not fully exfoliated and remained in a graphitic-like
15 state [38]. The oxygen-containing functional groups on the GO are mainly on the external
16 surface of the nanoparticles. This result is in line with the specification of GO nanoparticles
17 purchased that have 15-20 sheets and 4-10% edge-oxidized. After chemical reduction, this peak
18 remained in the CA-[BMIM]Cl-rGO nanofibers, as expected.



1

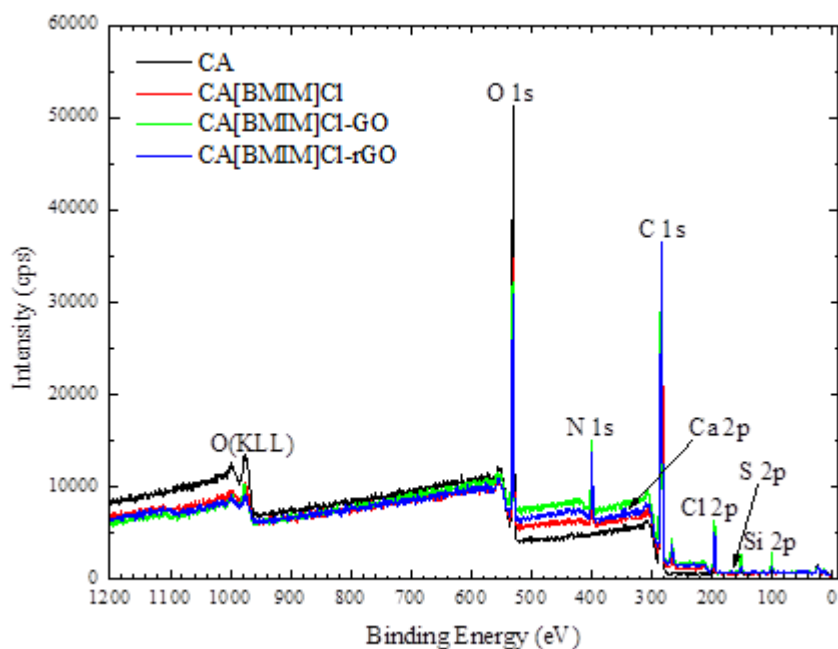
2 **Figure 4** (a) XRD patterns; (b) Raman spectra and (c) FTIR spectra of CA nanofibers, hybrid
 3 CA-[BMIM]Cl, CA-[BMIM]Cl-GO and CA-[BMIM]Cl-rGO nanofibers (GO conc. 0.43 wt%
 4 for the latter two samples).

5 To examine the influence of chemical reduction on the chemical structure of GO in more detail,
 6 the samples were studied by Raman spectroscopy, as shown in Figure 4b. The Raman spectra
 7 of CA-[BMIM]Cl-GO and CA-[BMIM]Cl-rGO both showed two bands at 1350 cm^{-1} and 1585
 8 cm^{-1} . These can be assigned to the D and G bands of the carbon materials, respectively [39,
 9 40]. The G band represents sp^2 -hybridized C-C bonds in a 2D hexagonal lattice, while the D
 10 band corresponds to the defects and disorder on the two-dimensional amorphization of the
 11 carbon network [41, 42]. These two peaks reveal that the graphene sheets of the GO have a

1 significant proportion of carbon disordered away from a perfect 2D hexagonal lattice. More
2 specifically, comparison of the CA-[BMIM]Cl-GO and CA-[BMIM]Cl-rGO spectra shows
3 that the D and G bands of CA-[BMIM]Cl-rGO nanofibers are more pronounced after chemical
4 reduction, where the spectrum shows less signals from surface functional groups. The relative
5 intensity of the G and D bands does not change significantly, supporting the evidence provided
6 by XRD that graphene sheets in the GO particles were not fully exfoliated showing sp²-
7 hybridized C-C bonds in a 2D hexagonal lattice and having sheet spacing close to the 0.33 nm
8 of graphite. Importantly, the chemical reduction did not significantly alter the stacking of the
9 graphene sheets, but modified the surface functional groups through deoxygenation [43-46].

10 *3.3 Chemical bonds and their interactions within the hybrid nanofibers*

11 The structure and interactions of each component in the hybrid nanofibers were revealed by
12 Raman, FTIR and XPS giving insights into the reason for the enhancement in conductivity. As
13 aforementioned, the Raman spectra of CA, CA-[BMIM]Cl, CA-[BMIM]Cl-GO and CA-
14 [BMIM]Cl-rGO are shown in Figure 4b, whereas the FTIR and XPS spectra are presented in
15 Figures 4c and 5, respectively. The Raman spectra of CA and CA-[BMIM]Cl showed the
16 asymmetric stretching vibration of the C-O-C glycosidic bond at 1121 cm⁻¹ and the pyranose
17 ring at 1080 cm⁻¹ with the presence of C-OH at 1265 cm⁻¹. The bands at 1736, 1435, and
18 1382 cm⁻¹ are attributed to the carbonyl group (C=O) and symmetric and asymmetric
19 vibrations of C-H, respectively, in the acetyl group [47-49]. More interestingly, the [BMIM]Cl
20 cation is observed in the CA-[BMIM]Cl sample with bands at 601 and 627 cm⁻¹. The intensities
21 show the co-existence of gauche and trans conformations of the IL [50, 51]. It is worth noting
22 that the inclusion of GO has resulted in the disappearance of most of the vibrational bands from
23 the Raman spectra of the corresponding hybrid nanofibers.

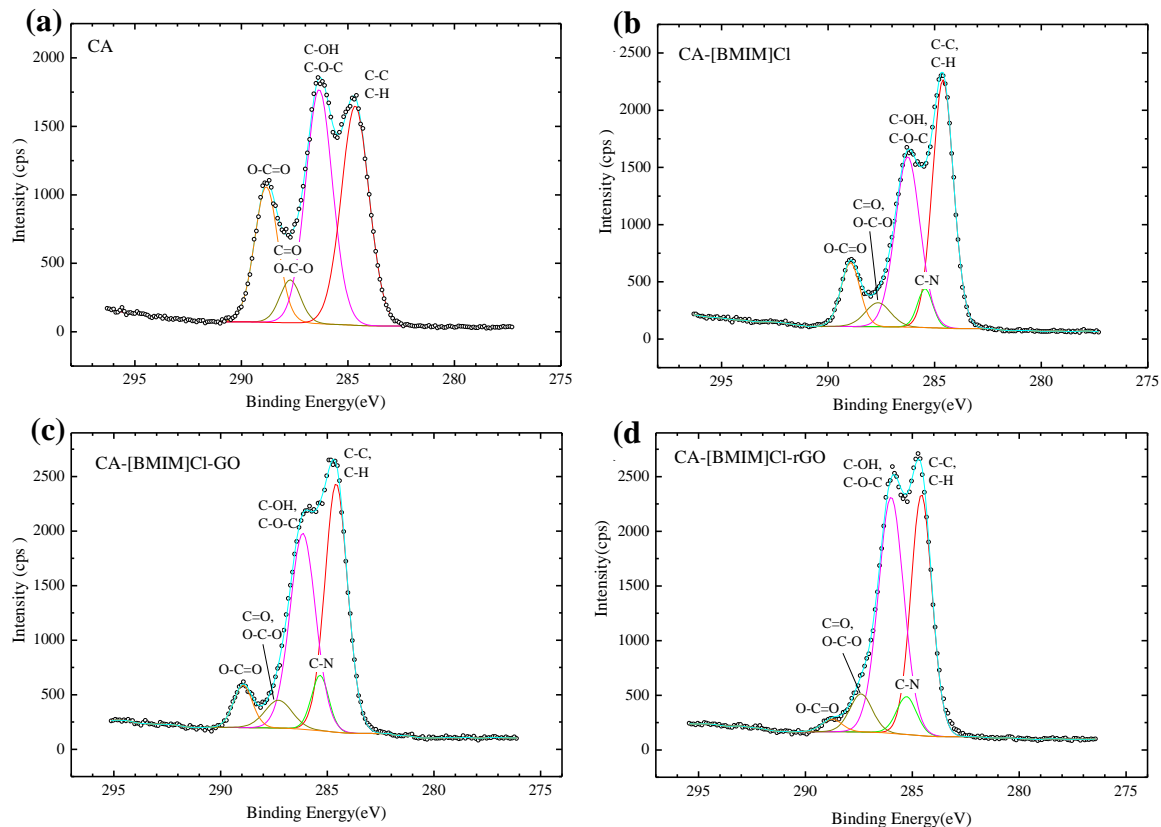


1

2 **Figure 5** XPS survey spectra of CA (black), CA-[BMIM]Cl (red), CA-[BMIM]Cl-GO (green),
 3 CA-[BMIM]Cl-rGO (GO conc. 0.43 wt%, blue).

4 The FTIR spectra of pure CA, CA-[BMIM]Cl and CA-[BMIM]Cl-rGO nanofibers in Figure
 5 4c show that pure CA nanofibers exhibited characteristic bands at 1735 cm^{-1} and 1367 cm^{-1}
 6 corresponding to C=O and C-H stretching from $-\text{OCOCH}_3$, respectively. Bands at 1220 cm^{-1}
 7 and 1030 cm^{-1} reveal the C-C and C-O stretching vibrations in the pyranoid ring and C-O-C
 8 (ether linkage) from the glycosidic units. In the CA-[BMIM]Cl spectrum, characteristic bands
 9 at 1746 cm^{-1} (C=C stretching), 1214 cm^{-1} (C=N stretching) and 1041 cm^{-1} (C-O stretching)
 10 indicate that the BMIM^+ and Cl^- ions of [BMIM]Cl formed hydrogen bonds with CA, as
 11 expected. The FTIR spectrum of CA-[BMIM]Cl-GO is similar to that of CA-[BMIM]Cl while
 12 the spectrum of [BMIM]Cl-rGO shows two new bands at 1659 cm^{-1} and 3229 cm^{-1} suggesting
 13 strong interactions (hydrogen bonding) between the carboxylic ($-\text{COOH}$) groups of graphene
 14 and carbonyl (C=O) groups of CA.

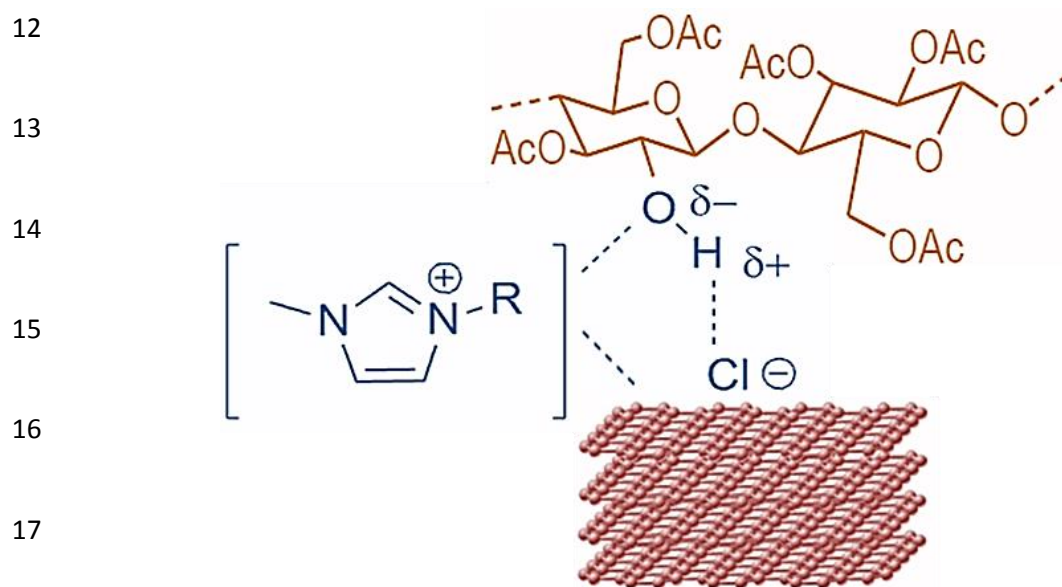
15



1
 2 **Figure 6** The C1s XPS spectra of (a) pristine CA nanofibers, (b) CA-[BMIM]Cl, (c) CA-
 3 [BMIM]Cl-GO, and (d) CA-[BMIM]Cl-rGO (GO conc. 0.43 wt%).

4 XPS was used to further examine the differences in chemical functionality in the hybrid
 5 nanofibers (Figure 5). The survey spectrum of pure CA nanofibers exhibits only two distinct
 6 peaks: C 1s at ~285 eV and O 1s at ~532 eV (Figure 5), while Cl 2p and N 1s peaks are present
 7 in all other spectra, confirming the presence of [BMIM]Cl. High resolution C 1s spectra were
 8 analyzed by monochromatic Al K α X-ray source ($h\nu = 1486.6$ eV). Each spectrum has been
 9 deconvoluted into five distinct peaks, as shown in Figure 6a-d for the nanofibers of pure CA,
 10 CA-[BMIM]Cl, CA-[BMIM]Cl-GO and CA-[BMIM]Cl-rGO, respectively. The sharp peak
 11 centered at 284.6 eV corresponds to C-C bonding and the relatively broad peak around
 12 286.1 eV is attributed to three different functional groups: hydroxyl (C-O); carbonyl (C=O)
 13 and imine (C-N). More specifically, the peaks in this region at 285.5, 285.7, 286.6 and 287.8 eV
 14 are attributed to carbon atoms in C-N, C=N, C-O, C=O, respectively. In the CA-[BMIM]Cl-

1 rGO nanofibers, the peak centered at 288.9 eV comes from the carboxyl group [C(O)O].
2 Comparing the C 1s XPS spectra (Figure 6a and b), it can be seen that the addition of
3 [BMIM]Cl significantly lowers the relative peak intensity of the oxygen-containing functional
4 groups from CA, and introduces a new peak attributed to C-N from [BMIM]Cl. The
5 introduction of GO results in some small changes in the relative peak intensities (comparing
6 Figure 6b and c). After the reduction of the CA-[BMIM]Cl-GO nanofibers, the C 1s spectrum
7 of the CA-[BMIM]Cl-rGO (Figure 6d) shows a dramatic decrease of the carboxyl peak. These
8 changes suggest that the hydrazine vapor step has indeed reduced the carboxyl groups in GO,
9 but may have also partially reduced CA, while the peak intensity of the other oxygen-
10 containing functional groups slightly increased. It is noteworthy to state that it has been shown
11 elsewhere that it is not yet possible to reduce GO completely by chemical reduction [44].



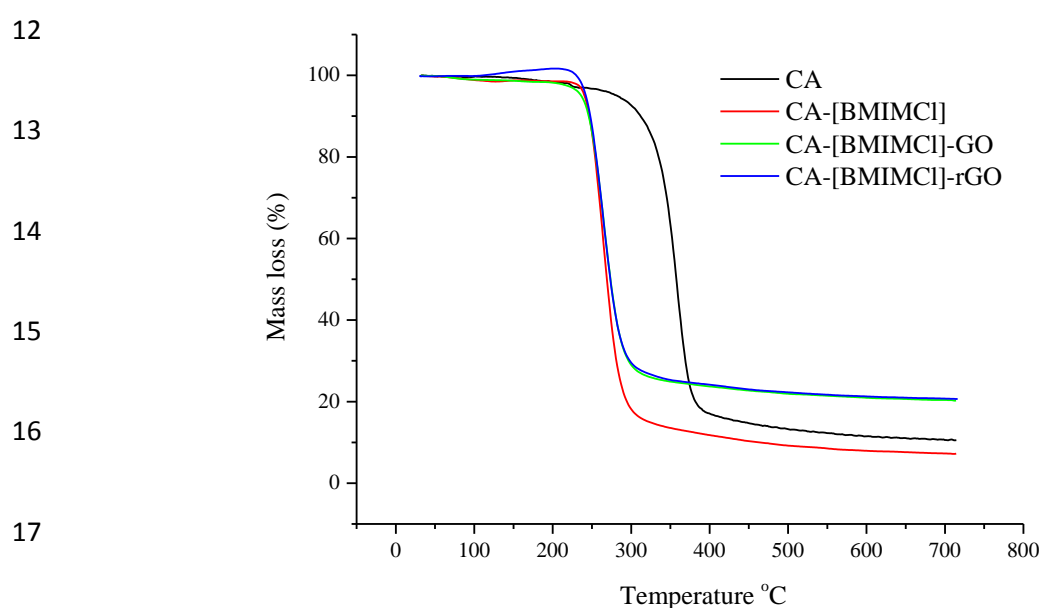
19 **Figure 7** Schematic illustration of the suggested interaction of graphene with CA and
20 [BMIM]Cl.

21 The proposed interactions of stacked graphene sheets with CA and [BMIM]Cl are
22 schematically shown in Figure 7. Removal of carboxyl groups and formation of more hydroxyl

1 groups may promote the formation of hydrogen-bonds with dissociated BMIM^+ and Cl^- ions
2 through unsubstituted hydroxyl functional groups in both GO and CA [52, 53]. The π -electrons
3 in the imidazole ring of BMIM^+ may interact with the rich π -electron clouds of the graphene
4 rings resulting in some delocalization and enhanced electrical conductivity.

5 3.4 Thermal analysis of the hybrid nanofibers

6 TGA has been carried out under argon to further examine the thermal stability and chemical
7 bonding differences in CA, CA-[BMIM]Cl, CA-[BMIM]Cl-GO and CA-[BMIM]Cl-rGO
8 nanofibers. These weight loss profiles (Figure 8) show that pure CA is more stable than the
9 composites. Pure CA decomposes in the range of 330 - 375°C with a corresponding weight
10 loss of approximately 82 wt%. In contrast, the addition of [BMIM]Cl lowers the decomposition
11 temperature range to 240 - 290°C with a corresponding weight loss of 85%.



19 **Figure 8** TGA profiles of pure CA (black), CA-[BMIM]Cl nanofibers (red), CA-[BMIM]Cl-
20 GO nanofibers (green) and CA-[BMIM]Cl-rGO nanofibers (blue).

1 The addition of 0.43% GO did not cause significant change in the decomposition temperature
2 but does decrease the weight loss to ~75%. Reduction using hydrazine does not cause any
3 identifiable changes in thermal decomposition nor char formation. These findings confirm that
4 the ionic liquid has fully separated CA molecular chains with no CA H-bonding following
5 mechanical mixing. This separation lowers the thermal stability of the CA by approximately
6 90°C. The addition of 0.43% GO does not affect the thermal stability of the CA, but introduced
7 an effective mass transfer barrier and char formation nucleus, resulting in an increased amount
8 of char formed. Such an enhancement could suggest that the graphene pallets were well aligned
9 during extrusion and spinning. The morphology, crystal structure, chemical bonding and
10 thermal analysis of the CA-[BMIM]Cl-GO nanofibers show that graphene stacks have been
11 successfully incorporated into CA nanofibers by dispersing GO in a [BMIM]Cl ionic liquid.
12 Polar functional groups, such as $-C=O$, $-COOH$ and $-OH$ on GO have not only assisted its
13 dispersion in the ionic liquid, but also facilitate strong and uniform interactions with CA in the
14 hybrid nanofibers. The well-dispersed and strongly bonded system allowed the graphene stacks
15 to form a continuous conductive network, achieving a drastic enhancement in electrical
16 conductivity after reduction using hydrazine, similar to the polystyrene-GO system reported by
17 Wu *et al.* [54]. These insights demonstrate that this new graphene-based hybrid nanocomposite
18 is a promising candidate for smart and flexible electronic and bio-electronic applications,
19 particularly in those systems which require high electrical conductivity.

20 **4. Conclusions**

21 In summary, a new method of exploiting a [BMIM]Cl ionic liquid for the fabrication of
22 graphene-based, bio-inspired (cellulose acetate) conductive CA-[BMIM]Cl-GO nanofibers
23 through electrospinning has been introduced. Combining the advantages of both GO and
24 [BMIM]Cl materials allowed a homogeneous dispersion of GO and better solubility of CA to

1 be achieved. The modest incorporation of 0.43% graphene oxide into the hybrid material
2 greatly enhanced the conductivity of the nanofiber mats by more than four orders of magnitude
3 to 5.30×10^{-3} S/cm. The uniform nanostructure of graphite oxide and BMIM in CA nanofibers
4 forms the conductive paths, which has been enhanced by chemical reduction of hydrazine via
5 an ultrasonic process. Such a facile strategy for the fabrication of bio-based, ultrathin,
6 lightweight, flexible nanofibers could open a new avenue towards sustainable material
7 development in the quest for high-performance next-generation smart electronic devices.

8 **Acknowledgements**

9 This work was supported by Estonian Academy of Science, Estonian Research Council
10 (IUT19-4) and by the European Regional Development Fund project TK141 “Advanced
11 materials and high-technology devices for energy recuperation systems.” The authors
12 acknowledge the Estonian Ministry of Education under institutional research financing IUT
13 19-28 and the European Union through the European Regional Development Fund. The authors
14 are also grateful for the financial support from the Estonian PhD allowance and Estonian
15 Ministry of Education and Research to support for this research at Tallinn University of
16 Technology Tallinn Estonia. Finally, KJ and PDT thank Christian Burton at Aston University
17 for assistance with physical characterization of the nanofibrous mats.

18 **References**

- 19 [1] Schiffman JD, Schauer CL. A Review: Electrospinning of Biopolymer Nanofibers and their
20 Applications. *Polymer Reviews*. 2008;48(2):317-52.
21 [2] Subbiah T, Bhat GS, Tock RW, Parameswaran S, Ramkumar SS. Electrospinning of nanofibers.
22 *Journal of Applied Polymer Science*. 2005;96(2):557-69.
23 [3] Ramakrishna S, Fujihara K, Teo W-E, Yong T, Ma Z, Ramaseshan R. Electrospun nanofibers:
24 solving global issues. *Materials Today*. 2006;9(3):40-50.
25 [4] Baji A, Mai Y-W, Wong S-C, Abtahi M, Chen P. Electrospinning of polymer nanofibers: Effects
26 on oriented morphology, structures and tensile properties. *Composites Science and Technology*.
27 2010;70(5):703-18.
28 [5] Chronakis IS, Grapenson S, Jakob A. Conductive polypyrrole nanofibers via electrospinning:
29 Electrical and morphological properties. *Polymer*. 2006;47(5):1597-603.

- 1 [6] Isakova A, Efremova O, Pullan N, Luer L, Topham PD. Design, synthesis and RAFT
2 polymerisation of a quinoline-based monomer for use in metal-binding composite microfibers. RSC
3 Advances. 2016;6(8):6598-606.
- 4 [7] Wang L, Wang M, Topham PD, Huang Y. Fabrication of magnetic drug-loaded polymeric
5 composite nanofibres and their drug release characteristics. RSC Advances. 2012;2(6):2433-8.
- 6 [8] Huang Z-M, Zhang YZ, Kotaki M, Ramakrishna S. A review on polymer nanofibers by
7 electrospinning and their applications in nanocomposites. Composites Science and Technology.
8 2003;63(15):2223-53.
- 9 [9] Wahab IF, Razak SIA, Azmi NS, Dahli FN, Yusof AHM, Nayan NHM. Electrospun Graphene
10 Oxide-Based Nanofibres. In: Silva AMT, Carabineiro SAC, eds. Advances in Carbon Nanostructures.
11 Rijeka: InTech 2016, p. Ch. 05.
- 12 [10] Mahdieh ZM, Mottaghitalab V, Piri N, Haghi AK. Conductive chitosan/multi walled carbon
13 nanotubes electrospun nanofiber feasibility. Korean Journal of Chemical Engineering.
14 2012;29(1):111-9.
- 15 [11] Gouda M, Abu-Abdeen M. Highly conductive cellulosic nanofibers for efficient water
16 desalination. Fibers and Polymers. 2017;18(11):2111-7.
- 17 [12] Yang T, Wu D, Lu L, Zhou W, Zhang M. Electrospinning of polylactide and its composites with
18 carbon nanotubes. Polymer Composites. 2011;32(8):1280-8.
- 19 [13] Hu K, Kulkarni DD, Choi I, Tsukruk VV. Graphene-polymer nanocomposites for structural and
20 functional applications. Progress in Polymer Science. 2014;39(11):1934-72.
- 21 [14] Chee WK, Lim HN, Zainal Z, Huang NM, Harrison I, Andou Y. Flexible Graphene-Based
22 Supercapacitors: A Review. The Journal of Physical Chemistry C. 2016;120(8):4153-72.
- 23 [15] Meng F, Lu W, Li Q, Byun J-H, Oh Y, Chou T-W. Graphene-Based Fibers: A Review. Advanced
24 Materials. 2015;27(35):5113-31.
- 25 [16] Peng R, Wang Y, Tang W, Yang Y, Xie X. Progress in Imidazolium Ionic Liquids Assisted
26 Fabrication of Carbon Nanotube and Graphene Polymer Composites. Polymers. 2013;5(2):847.
- 27 [17] Marsh KN, Boxall JA, Lichtenhaler R. Room temperature ionic liquids and their mixtures—a
28 review. Fluid Phase Equilibria. 2004;219(1):93-8.
- 29 [18] Swatloski RP, Spear SK, Holbrey JD, Rogers RD. Dissolution of Cellulose with Ionic Liquids.
30 Journal of the American Chemical Society. 2002;124(18):4974-5.
- 31 [19] Meli L, Miao J, Dordick JS, Linhardt RJ. Electrospinning from room temperature ionic liquids
32 for biopolymer fiber formation. Green Chemistry. 2010;12(11):1883-92.
- 33 [20] Viswanathan G, Murugesan S, Pushparaj V, Nalamasu O, Ajayan PM, Linhardt RJ. Preparation
34 of Biopolymer Fibers by Electrospinning from Room Temperature Ionic Liquids. Biomacromolecules.
35 2006;7(2):415-8.
- 36 [21] Xie H, Zhang S, Li S. Chitin and chitosan dissolved in ionic liquids as reversible sorbents of
37 CO₂. Green Chemistry. 2006;8(7):630-3.
- 38 [22] Javed K, Krumme A, Krasnou I, Mikli V, Viirsalu M, Plamus T, et al. Impact of 1-butyl-3-
39 methylimidazolium chloride on the electrospinning of cellulose acetate nanofibers. Journal of
40 Macromolecular Science, Part A. 2017:1-6.
- 41 [23] Zavgorodnya O, Shamshina JL, Bonner JR, Rogers RD. Electrospinning Biopolymers from Ionic
42 Liquids Requires Control of Different Solution Properties than Volatile Organic Solvents. ACS
43 Sustainable Chemistry & Engineering. 2017;5(6):5512-9.
- 44 [24] Zhang G, Sun M, Liu Y, Liu H, Qu J, Li J. Ionic Liquid Assisted Electrospun Cellulose Acetate
45 Fibers for Aqueous Removal of Triclosan. Langmuir. 2015;31(5):1820-7.
- 46 [25] Freire MG, Teles ARR, Ferreira RAS, Carlos LD, Lopes-da-Silva JA, Coutinho JAP. Electrospun
47 nanosized cellulose fibers using ionic liquids at room temperature. Green Chemistry.
48 2011;13(11):3173-80.
- 49 [26] He C, Sun S, Peng H, Tsui CP, Shi D, Xie X, et al. Poly(ionic liquid)-assisted reduction of
50 graphene oxide to achieve high-performance composite electrodes. Composites Part B: Engineering.
51 2016;106:81-7.

- 1 [27] Lyu Q, Yan H, Li L, Chen Z, Yao H, Nie Y. Imidazolium Ionic Liquid Modified Graphene Oxide:
2 As a Reinforcing Filler and Catalyst in Epoxy Resin. *Polymers*. 2017;9(9):447.
- 3 [28] Peng H, Meng L, Niu L, Lu Q. Simultaneous Reduction and Surface Functionalization of
4 Graphene Oxide by Natural Cellulose with the Assistance of the Ionic Liquid. *The Journal of Physical
5 Chemistry C*. 2012;116(30):16294-9.
- 6 [29] Gudkova V, Krumme A, Märtson T, Rikko M, Tarasova E, Savest N, et al. 1-butyl-3-
7 methylimidazolium chloride assisted electrospinning of SAN/MWCNTs conductive reinforced
8 composite membranes. *Journal of Electrostatics*. 2015;78:11-6.
- 9 [30] Huddleston JG, Visser AE, Reichert WM, Willauer HD, Broker GA, Rogers RD. Characterization
10 and comparison of hydrophilic and hydrophobic room temperature ionic liquids incorporating the
11 imidazolium cation. *Green Chemistry*. 2001;3(4):156-64.
- 12 [31] Wang Z, Wu S, Zhang J, Chen P, Yang G, Zhou X, et al. Comparative studies on single-layer
13 reduced graphene oxide films obtained by electrochemical reduction and hydrazine vapor reduction.
14 *Nanoscale Research Letters*. 2012;7(1):161.
- 15 [32] Youn SC, Geng J, Son BS, Yang SB, Kim DW, Cho HM, et al. Effect of the Exposure Time of
16 Hydrazine Vapor on the Reduction of Graphene Oxide Films. *Journal of Nanoscience and
17 Nanotechnology*. 2011;11(7):5959-64.
- 18 [33] Fendt S, Padmanabhan S, Blanch HW, Prausnitz JM. Viscosities of Acetate or Chloride-Based
19 Ionic Liquids and Some of Their Mixtures with Water or Other Common Solvents. *Journal of Chemical
20 & Engineering Data*. 2011;56(1):31-4.
- 21 [34] Tripathi SN, Rao GSS, Mathur AB, Jasra R. Polyolefin/graphene nanocomposites: a review.
22 *RSC Advances*. 2017;7(38):23615-32.
- 23 [35] Dharaskar SA, Varma MN, Shende DZ, Yoo CK, Wasewar KL. Synthesis, Characterization and
24 Application of 1-Butyl-3 Methylimidazolium Chloride as Green Material for Extractive Desulfurization
25 of Liquid Fuel. *The Scientific World Journal*. 2013;2013:9.
- 26 [36] Zhao X, Zhang Q, Chen D, Lu P. Enhanced Mechanical Properties of Graphene-Based
27 Poly(vinyl alcohol) Composites. *Macromolecules*. 2010;43(5):2357-63.
- 28 [37] Bao C. Cellulose acetate / plasticizer systems : structure, morphology and dynamics.
29 Université Claude Bernard Lyon 1, PhD thesis, 2015.
- 30 [38] Yuan Q. Intumescent Mechanisms of Fire-retarding polyurethane systems and development
31 of graphite/polymer nano-composites. 2004.
- 32 [39] Claramunt S, Varea A, López-Díaz D, Velázquez MM, Cornet A, Cirera A. The Importance of
33 Interbands on the Interpretation of the Raman Spectrum of Graphene Oxide. *The Journal of Physical
34 Chemistry C*. 2015;119(18):10123-9.
- 35 [40] Jorio A, Ferreira EHM, Moutinho MVO, Stavale F, Achete CA, Capaz RB. Measuring disorder
36 in graphene with the G and D bands. *physica status solidi (b)*. 2010;247(11-12):2980-2.
- 37 [41] Malard LM, Pimenta MA, Dresselhaus G, Dresselhaus MS. Raman spectroscopy in graphene.
38 *Physics Reports*. 2009;473(5-6):51-87.
- 39 [42] Kudin KN, Ozbas B, Schniepp HC, Prud'homme RK, Aksay IA, Car R. Raman Spectra of
40 Graphite Oxide and Functionalized Graphene Sheets. *Nano Letters*. 2008;8(1):36-41.
- 41 [43] Park S, An J, Jung I, Piner RD, An SJ, Li X, et al. Colloidal suspensions of highly reduced
42 graphene oxide in a wide variety of organic solvents. *Nano Letters*. 2009;9(4):1593-7.
- 43 [44] Stankovich S, Dikin DA, Piner RD, Kohlhaas KA, Kleinhammes A, Jia Y, et al. Synthesis of
44 graphene-based nanosheets via chemical reduction of exfoliated graphite oxide. *Carbon*.
45 2007;45(7):1558-65.
- 46 [45] Shilpa, Basavaraja BM, Majumder SB, Sharma A. Electrospun hollow glassy carbon-reduced
47 graphene oxide nanofibers with encapsulated ZnO nanoparticles: a free standing anode for Li-ion
48 batteries. *Journal of Materials Chemistry A*. 2015;3(10):5344-51.
- 49 [46] Yao S, Li Y, Zhou Z, Yan H. Graphene oxide-assisted preparation of poly(vinyl alcohol)/carbon
50 nanotube/reduced graphene oxide nanofibers with high carbon content by electrospinning
51 technology. *RSC Advances*. 2015;5(111):91878-87.

- 1 [47] Duverger C, Nedelec JM, Benatsou M, Bouazaoui M, Capoen B, Ferrari M, et al. Waveguide
2 Raman spectroscopy: a non-destructive tool for the characterization of amorphous thin films.
3 *Journal of Molecular Structure*. 1999;480-481:169-78.
- 4 [48] J. A. Sánchez-Márquez RF-R, I. Cano-Rodríguez, Z. Gamiño-Arroyo, E. Rubio-Rosas, J. M.
5 Kenny, N. Rescignano. Membrane Made of Cellulose Acetate with Polyacrylic Acid Reinforced with
6 Carbon Nanotubes and Its Applicability for Chromium Removal. *International Journal of Polymer*
7 *Science*. 2015;2015:12.
- 8 [49] Scherer JR, Bailey GF, Kint S, Young R, Malladi DP, Bolton B. Water in polymer membranes
9 raman scattering from cellulose acetate films. *The Journal of Physical Chemistry*. 1985;89(2):312-9.
- 10 [50] Satoshi H, Ryosuke O, Hiro-o H. Raman Spectra, Crystal Polymorphism, and Structure of a
11 Prototype Ionic-liquid [bmim]Cl. *Chemistry Letters*. 2003;32(6):498-9.
- 12 [51] Mizuno K, Imafuji S, Ochi T, Ohta T, Maeda S. Hydration of the CH Groups in Dimethyl
13 Sulfoxide Probed by NMR and IR. *The Journal of Physical Chemistry B*. 2000;104(47):11001-5.
- 14 [52] Isik M, Sardon H, Mecerreyes D. Ionic Liquids and Cellulose: Dissolution, Chemical
15 Modification and Preparation of New Cellulosic Materials. *International Journal of Molecular*
16 *Sciences*. 2014;15(7):11922-40.
- 17 [53] Gross AS, Bell AT, Chu J-W. Thermodynamics of Cellulose Solvation in Water and the Ionic
18 Liquid 1-Butyl-3-Methylimidazolium Chloride. *The Journal of Physical Chemistry B*.
19 2011;115(46):13433-40.
- 20 [54] Wu N, She X, Yang D, Wu X, Su F, Chen Y. Synthesis of network reduced graphene oxide in
21 polystyrene matrix by a two-step reduction method for superior conductivity of the composite.
22 *Journal of Materials Chemistry*. 2012;22(33):17254-61.

23

24

25